Additive Manufacturing 59 (2022) 103142

Contents lists available at ScienceDirect

Additive Manufacturing

journal homepage: www.elsevier.com/locate/addma

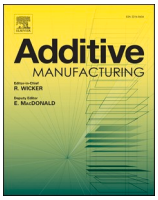

Novel post-processing procedure to enhance casting molds manufactured by binder jetting AM

P. Rodríguez-González [a], P. Zapico [b,*], P.E. Robles-Valero [a], J. Barreiro [a]

[a] Department of Mechanical, Informatics and Aerospace Engineering, University of León, Campus de Vegazana, 24071 León, Spain
[b] Department of Construction and Manufacturing Engineering, University of Oviedo, Campus of Gijón, 33204 Gijón, Spain

ARTICLE INFO

Keywords:
Calcium sulfate
Epsom salt
Vacuum infiltration
Binder jetting
Casting expendable elements

ABSTRACT

The significant improvements made in additive manufacturing (AM) techniques since their beginnings, coupled with its intrinsic advantages, have resulted in a technology that stands out as most suitable for applications in leading sectors today. In addition to some of the properties of the parts, there are also some inherent aspects of AM techniques that hinder their applicability. In this respect, the application of calcium sulfate parts manufactured by binder jetting (BJ), as expendable casting elements, is limited by both the high quantity of volatile substances, due to the BJ process, and their low compression resistance. In this work, a novel part post-processing procedure is presented. This procedure consists of applying various heat treatments, in combination with a vacuum infiltration process using an Epsom salt solution. The procedure reduces the volatile content of BJ AM parts and enhances the compression strength with little modification to the part geometry. This post-processing substantially improves the applicability of BJ AM parts as expendable casting elements. After presenting this novel procedure and analyzing the significant enhancement of the properties of the AM calcium sulfate parts (i.e. permeability, the reduction of volatile content and reduction of compressive strength), a case study is presented with an expendable mold for aluminum casting. This procedure allows for a safer casting process, improves the part's surface quality and reduces the internal porosity of the cast parts.

1. Introduction

Additive manufacturing began to develop in the 1980 s. At that time, it was named rapid prototyping and consisted of a set of techniques that allowed parts to be manufactured quickly and easily from their digital models, by means of adding layers of material [1,2]. The development of new techniques, the use of new materials and the application of new post-processing procedures to the manufactured parts, improved the properties of the products, allowing these sets of techniques to be referred to as a technology in their own right: Additive Manufacturing (AM). The main advantage of AM is the high degree of product customization and complexity it allows without significantly increasing the cost, which enables mass production of individual customized parts [3]. In addition, the AM enables quicker new product development, with low or no redesign penalty, as well as improving supply chain efficiency thanks to a decentralized and on-demand manufacturing [4]. Despite the design demands of some of these techniques [5], as well as the need to use models to optimize parts quality [6], AM is of great interest to several leading industrial sectors such as aerospace, automotive and medical.

One of the AM techniques that has received the most attention in recent years is known as Binder Jetting (BJ), based on conglomerating powder particles by means of a binding substance [7–10]. This technique can be applied to different materials such as calcium sulfate, silica, or alumina [11–13]. As an additive manufacturing process, this technique consists of the consecutive deposition of the different layers in which the digital model of the part has been previously sliced. The deposition of each layer begins by spreading a layer of powder on a platform using a scraper or a roller. Then, by means of a print head, micro-droplets of a binding substance are selectively projected on the positions where the powder particles need to be bonded, i.e. the area inside the perimeters belonging to the corresponding layer, obtained by the previous slicing of the digital model. This allows the conglomeration of the powder reached by the binder, forming a thin layer with the desired geometry. The platform is then lowered by a distance equivalent to the layer thickness used in the slicing. This process is repeated for successive layers in which the part model was sliced. After manufacturing all of the layers, a three-dimensional part is obtained that

* Corresponding author.
E-mail address: zapicopablo@uniovi.es (P. Zapico).

https://doi.org/10.1016/j.addma.2022.103142
Received 1 March 2022; Received in revised form 25 August 2022; Accepted 7 September 2022
Available online 10 September 2022

can be considered as a green part, in an as-built condition. Usually, different post-processing procedures are applied to this initial part, to improve the superficial finishing and/or its properties [14,15].

Although BJ has been successfully applied in sectors as diverse as aeronautics [16] and biomedicine [17–19], much effort is now being devoted to applying it to the foundry industry because of the time and cost reductions it can enable [20]. Chen et al. [21] reviewed the AM techniques used for ceramic materials, highlighting BJ as the most suitable for manufacturing expendable molds and cores. Although metal casting is a technique that dates back to ancient times, its development still remains a challenge [22], mainly due to its low competitiveness when applied to short manufacturing series compared to other manufacturing processes, such as machining [23]. This lack of competitiveness could be overcome by using expendable elements obtained by additive manufacturing, given the great advantages in terms of design freedom, high complexity, low waste and material costs, as well as better supply chain efficiency than conventional casting techniques [24]. In this regard, Almaghariz et al. [25] identified batch size as a function of the geometrical complexity of the cast part such that, below it, the use of this AM technique for metal casting is more competitive than other processes. They stated the effectiveness of this symbiosis for batch sizes of 45 units to 1000 units, depending on the geometrical complexity of the manufactured part.

Despite the occasional success of the BJ application for metal casting, there are still certain challenges that limit its applicability in this field. The main issue is the higher amount of binder liquid required by this technique, compared to the amount of liquid used in the fabrication of conventional expendable molds [26]. The binders usually used in conventional techniques contain significant levels of furans (C_4H_4O), substances that are very harmful to health and the environment [27]. On the contrary, BJ uses harmless substances, primarily composed of water [11]. Nevertheless, the reduction of the volatile load of the molds obtained by this AM technique is still an important issue, given its negative effect on the quality of the molded parts. In this sense, Rodríguez-González et al. [28] highlighted the surface and internal defects of molded parts due to the expulsion of volatiles in the form of gas during the pouring of aluminum into expendable BJ molds made of calcium sulfate. Although a reduction in the amount of binder used during AM mold manufacturing might seem to be the ultimate solution to this problem, Vlasea et al. [29] demonstrated the high sensitivity of this technique to the amount of binder, by monitoring a specific parameter that they defined as *binder level*. This parameter is critical for the quality of the parts and the proper performance of the process. Manufacturing fails if it is too low, given the lack of cohesion between powder particles. On the contrary, if the binder level is too high, the dimensional quality is damaged due to bleeding of the injected traces on the powder bed [30]. Given the narrowness of the permissible variation range of binder level and the fact that it is a parameter that is not configurable in most commercial AM machines, it is interesting to develop procedures to reduce the volatile load of BJ molds once they have been manufactured, improving their applicability to metal casting. In addition, it should not be forgotten that these procedures could improve other interesting properties in this application. In this sense, some workers have achieved slight improvements in strength by using infiltration solutions such as magnesium sulfate diluted in distilled water [31,32]. Unfortunately, these efforts do not focus on the reduction of volatiles, have even increased their content due to the type of solutions used, so the development of specific post-processing procedures for manufacturing casting-focused elements is still an issue to be addressed, in order to improve the applicability of this technique. These post-processes could be applied with a hybrid approach [33], given the limitations of current BJ equipment in this respect.

This work presents a novel post-processing procedure for calcium sulfate parts, obtained by AM binder jetting techniques with calcium sulfate, and based on an infiltration process in combination with different thermal treatments, which improve the strength and reduce the volatile content of these parts. This substantially improves the applicability of this type of part as expendable elements, i.e. molds, cores, etc., in the casting process. After a description of the procedure, its application to different cubic specimens is presented to analyze the evolution of the material over the post-processing steps, in terms of weight, dimensions, apparent density, surface quality and compressive strength, due to the importance of these characteristics in the casting process. Finally, the procedure is applied to a case study consisting of an aluminum casting mold. The quality (in terms of roughness and porosity) of the part obtained using the AM mold, post-treated with the proposed procedure, is compared with those of a part obtained with an equivalent mold used after manufacturing without applying the presented post-processing procedure.

2. Infiltration and heat treatment procedure of AM gypsum parts

Plaster molds are made of plaster of Paris (gypsum or calcium sulfate), mixed with a small amount of additive. These molds are used to manufacture small, highly detailed parts with high dimensional accuracy and a good surface finish and, therefore, they are considered to be precision molds. These molds can be used in temperatures up to 1200 °C. Thus, they are often used to form plastic parts or low melting point metals and alloys, such as aluminum or zinc. Due to the low permeability of the gypsum, vacuum or pressure techniques are often applied during the pouring of the metal, to facilitate the evacuation of gases and properly fill the mold. In addition, this type of mold allows more homogeneous and equiaxial granular structures to be achieved because of the slow cooling rate derived from the low thermal conductivity of gypsum [34].

Nowadays, there are AM industrial machines that allow the manufacture of parts in calcium sulfate dehydrated gypsum ($CaSO_4 + 2{\cdot}H_2O$). For this purpose, a binder, which is basically composed of water, is projected on a bed of calcium sulfate hemihydrate powder. This produces an exothermic reaction known as setting of gypsum, as illustrated in Eq. (1). The problem with using these AM parts as molds lies in their low strength and high moisture content. This is something that also occurs in gypsum molds in general, in which case additives are mixed with the calcium sulfate hemihydrate powders to control the setting of the gypsum; different heat treatments (HT) are applied to the molds once they have been shaped, to control their moisture content. Both procedures also improve permeability [35]. In the case of molds made by AM, there is no supply of gypsum mixed with specific additives for casting, nor clear guidelines from manufacturers or suppliers for performing specific heat treatments for those parts that will work as molds or casting elements.

$$CaSO_4{\cdot}½H_2O + 1.5H_2O \rightarrow CaSO_4{\cdot}2H_2O + \text{Heat} \quad (1)$$

This type of part, obtained by AM, is largely gypsum and so designing a series of heat treatments to reduce the water content is preferrable. Therefore, controlling the temperature at which they are treated is critical in order to eliminate as much moisture as possible, without excessively damaging their strength, an essential characteristic for their applications in casting processes. The calcium sulfate dehydrate used by AM machines is obtained from gypsum by means of an endothermic reaction called calcination (2), which is inverse to the setting represented in Eq. (1). Depending on the ambient humidity to which gypsum is exposed during calcination, different phases of hemihydrate can be obtained: α-hemihydrate and β-hemihydrate. Both are obtained at 80 °C and above, the former in a humid environment and the latter in a dry environment. Although both have the same chemical composition ($CaSO_4{\cdot}½H_2O$), the former produces a more prismatic crystal structure than the latter, which gives the material greater strength. If the calcination temperature exceeds 170 °C, the material loses even more water and phases such as γ-anhydrite ($CaSO_4{\cdot}0.05H_2O$) or the anhydrous form ($CaSO_4$) appear. The latter has difficulties reacting with water and returns to a previous, more hydrated, state. In addition, the material

becomes even more brittle.

$$CaSO_4 \cdot 2H_2O + Heat \rightarrow CaSO_4 \cdot \tfrac{1}{2}H_2O + Steam \quad (2)$$

On the other hand, although the gypsum extracted from the AM machines in the form of green parts does not contain additives to control setting and improving its strength, these can be introduced into the parts after manufacturing using infiltration processes. In these processes, to use different sulfates such as magnesium or potassium sulfate [36] is interesting, due to the strength improvement effects in gypsum. Due to the low permeability showed by these parts, rather than spraying or immersing them in a water solution of these additives, as recommended by some manufacturers of these AM machines [37], it is interesting to apply them using vacuum infiltration processes to ensure deep penetration of the additives. These processes can be performed by immersing the parts in a bath of sulfate solution and applying a vacuum. In the case of using magnesium sulfate, one option is Epsom salts, consisting of magnesium sulfate heptahydrate ($MgSO_4 \cdot 7H_2O$). This colourless salt has a multitude of applications in several industrial sectors, such as fertilizers, cement, textiles and medicine. It is also used in the home because of its anti-inflammatory properties [38]. When using this sulfate, it is important to be aware of the effect that the application of thermal treatments (aimed at eliminating the humidity of the gypsum in which it has been infiltrated) may have on its structure. Magnesium sulfate heptahydrate is converted into its monohydrate form ($MgSO_4 \cdot H_2O$) with heat treatments up to 150 °C, changing it to its anhydrous form ($MgSO_4$) with treatments above 200 °C.

Once the properties and the effect of temperature on both the gypsum (of which the AM parts are composed) and on the magnesium sulfate (that improves the properties of the former for its use as casting molds) are known, a procedure to infiltrate this sulfate in the parts to improve their strength, by reducing their moisture content, is presented. This procedure consists of four steps:

1. First drying HT: as built AM part is held at 80 °C for 2 h to produce the gypsum calcination and remove most of the moisture picked up during the AM process. This moisture comes from the binder used during the manufacturing process. Then, the part is taken out of the furnace and cooled freely in the air to reach room temperature. This step allows the material to revert to the hemihydrate state and providing an optimal condition for further infiltration processes.
2. Infiltration: the part is immersed in a solution of magnesium sulfate in distilled water at maximum solubility (0.71 g/ml at 20 °C) in a vacuum chamber with 150 mbar absolute pressure applied for one minute. This step allows the solution to penetrate a great depth into the material, preventing it from acting only on the surface. After applying the vacuum during that time, and the subsequent depressurization, the part is removed from the chamber and the excess solution is removed using absorbent paper. After this infiltration, the hemihydrate reverts to its dehydrated state. In addition, magnesium sulfate heptahydrate will have been homogeneously diffused trough the volume of the AM part.
3. Capillary humidity removal HT: the part is held at 80 °C for 24 h. This allows removal of the excess capillary moisture, i.e. non-crystallization water, reverting the calcium sulfate to its hemihydrate state and removing part of the crystallization water contained in the magnesium sulfate. The removal of this excess of moisture is critical for the next step of the procedure, as will be discussed below.
4. Second drying HT: the part is held between 150 °C and 200 °C for 6 h. This allows the calcium sulfate to lose much of the water of crystallization, without generating an excess of γ-anhydrite phase and the magnesium sulfate is converted to a near-anhydrous state. These changes will occur to a greater extent, the higher the temperature used, within the temperature range cited above. Although this last phase reduces the mechanical properties of the material, it allows the removal of a large amount of moisture, which is vital for casting processes. Finally, it is important to remark that this last step must not be applied without having applied the previous one, *capillary humidity removal HT*, since the material would break due to the sudden elimination of a large amount of crystallization water in the form of steam.

Table 1
Project CJP 660Pro main specifications [39].

Specification	Units	Value
Net build volume (x, y, z)	mm	254, 381, 203
Color	–	Full CMYK
Resolution	DPI	600 × 540
Layer thickness	μm	102
Number of jets	–	1520
Number of print heads	–	5
Binder / Volume ratio of core*	%	12
Binder / Volume ratio of shell*	%	24

* At 100% of saturation

Table 2
Mechanical properties of VisiJet PXL infiltrated with *Eco-friendly and safe solution* [37].

Specification	ASTM Condition	Units	Value
Tensile Strength	D638	MPa	2.38
Elongation at break	D638	%	0.04
Flexural strength	D790	MPa	13.10
Flexural modulus	D790	MPa	6355
Modulus of elasticity	D638	MPa	12855

The HT and infiltration process holding times considered in this procedure may vary depending on the size of the AM part. The proposed holding times are suitable for mold-type parts which allow the production of aluminum parts between 100 and 1000 g. This is compatible with the usual size of expendable mold type parts that can be manufactured in common AM industrial machines available today. In the following sections, the changes that the material undergoes as a result of the application of each step of this procedure are analyzed in detail. Furthermore, a case study is applied to aluminum casting and analyzed.

3. Materials and methods

In this section the material means used in the research are presented, including the AM machine and the rest of the equipment used to apply the developed procedure and to evaluate the effect on the material. Subsequently, the methods used to both analyze the material properties of the cubic specimens in each step of the procedure and to demonstrate the advantages of using this procedure in case of aluminum casting, are presented.

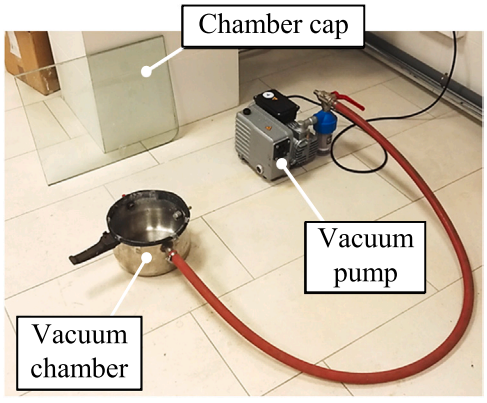

Fig. 1. Tailor-made infiltration system.

Table 3
AlSi7Mg composition according to the supplier.

Element	Al	Si	Fe	Mg	Mn	Ti	Cu	Ni	Pb	Sn	Zn
Weight (%)	Bal.	7.50	0.45	0.65	0.35	0.25	0.15	0.15	0.15	0.05	0.15

Table 4
Some properties of AlSi7Mg [43].

Specification	Units	Value
Density	kg/m^3	2650
Yield strength[a]	MPa	180
Ultimate strength[a]	MPa	220
Liquidus temperature	°C	603
Solidus temperature	°C	558
Thermal conductivity	w/(m·K)	150–170
Solidification shrinkage	%	7.14
Thermal expansion coefficient	10^{-6} K	22

[a] At T6 condition [b]From 293–373 K

3.1. Materials

In this work, the ProJet CJP 660Pro machine by 3D Systems was used [7]. The main specifications of this binder jetting machine are shown in Table 1. Visijet PXL Core of the same commercial brand was used as the powder material. This material consists of calcium sulfate hemihydrate or plaster of Paris powder of 80–90% purity, with an average particle size of 77 μm, a density of 2.6–2.7 g/cm^3, a melting point of 1450 °C and a water solubility of 0.83% [11]. To achieve the binding of the powder during the manufacturing process, this machine selectively injects droplets of binder liquid called VisiJet PXL on the powder bed. This binder, which is supplied by 3DSystems and consists of a 1% solution of 2-pyrrolidone (C_4H_7NO) in distilled water [39], causes the setting of the material transforming it in calcium sulfate dehydrate or gypsum. By repeating this process on successive layers of powder, the part is manufactured additively. With the aim of improving the mechanical properties of the parts, the manufacturer recommends the use of different infiltrate substances. One of them, considered Eco-friendly and safe, is a solution of Epsom salt in water [37]. This salt is magnesium sulfate heptahydrate and its maximum solubility in distilled water at 20 °C is 0.71 g/ml. This compound has different applications and is practically harmless to health and the environment; it is available from a multitude of suppliers. The infiltration procedure for this salt (recommended by the machine manufacturer) simply consists of spraying the part with a small amount of this solution [37]. After this process and a subsequent heat treatment, holding the part at 37.8 °C for 24 h, the material properties reach those shown in Table 2.

As explained above, the novel post-processing procedure presented in this paper consists of the combination of different heat treatments with an infiltration process using vacuum techniques. For the heat treatments, a Digiheat-TFT digital temperature-controlled furnace from Selecta, with a capacity of 150 l and a maximum temperature of 250 °C, was used. For the Epsom salt infiltration process, a 25-litre tailor-made vacuum chamber was used, connected to a vacuum pump capable of extracting a maximum flow rate of 24 m^3/h and reaching a minimum absolute pressure of 0.5 mbar, see Fig. 1. During the infiltration processes carried out in this work, a pressure of 150 mbar was reached in the vacuum chamber, measured with a Panasonic DP-101 vacuum sensor.

To evaluate changes in mass and density, a precision balance M-320 CBC (Cobos) was used, which allows hydrostatic weighing. These tests were carried out according to the three weights method recommended by ASTM C373–88 [40]. A 2-propanol with 99.9% purity was employed as an immersion liquid, avoiding the use of water due to the high solubility of the material. To analyze dimensional variations, a Mistral DEA Coordinate Measuring Machine was used. To analyze the surface quality, a roughness Surftest SJ-500 profilometer (by Mitutoyo) was used, configured with λ_c and λ_s of 2.5 mm and 8 μm, respectively, following

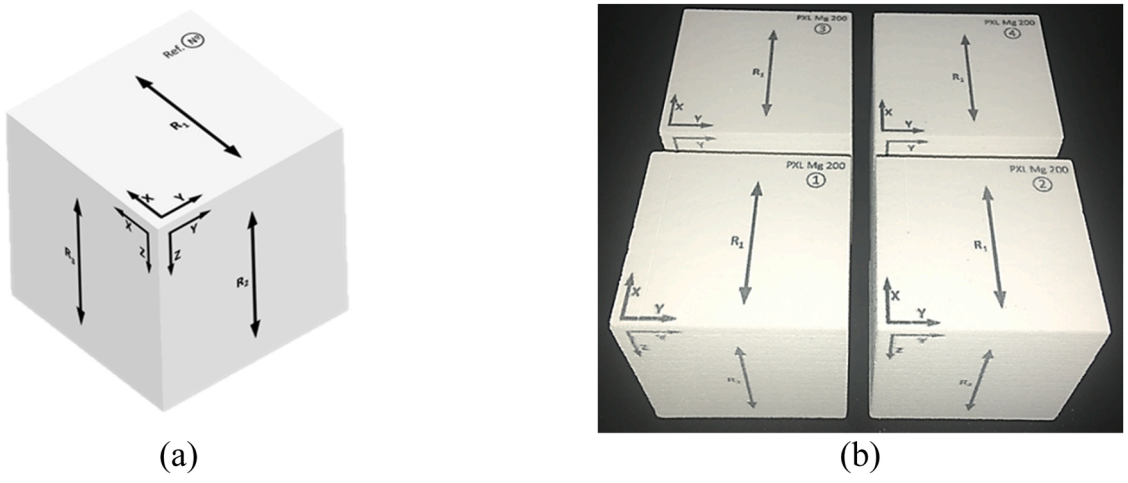

Fig. 2. Specimen cubes used: (a) model, (b) set of as-built cubes.

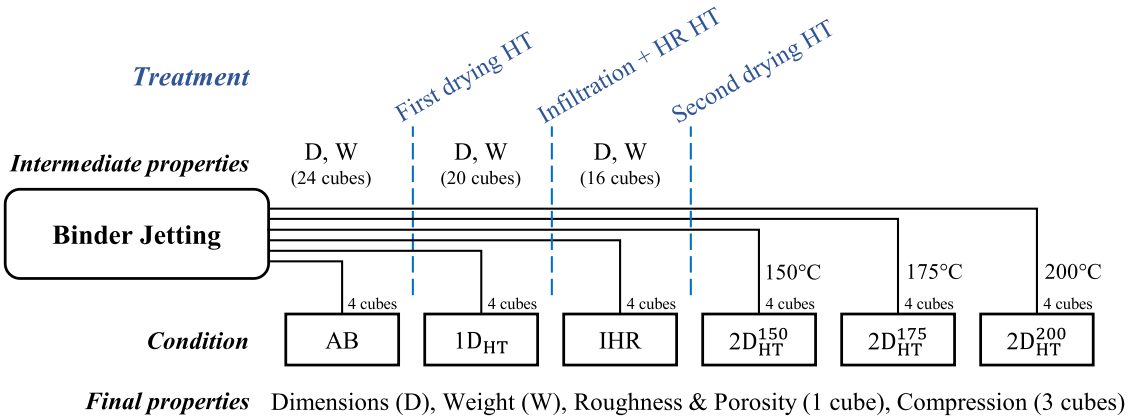

Fig. 3. Cube specimens treatment procedure and intermediate/final properties tested.

ISO 4288 recommendations [41]. Finally, to evaluate the compressive strength of the material in the different conditions reached during the post-processing, a universal ME-402 machine (by Servosis) equipped with a 50 kN load cell was used. These tests followed the recommendations of the ISO 679 standard [42].

To validate the novel post-processing procedure presented, a case study was carried out, consisting of the casting of an AlSi7Mg aluminum alloy [43] using an expendable mold obtained by BJ AM technique and treated with the presented procedure. The composition and main specifications of this alloy are shown in Table 3 and Table 4.

The casting of this aluminum was carried out by gravity, after melting it using an induction furnace model Agatronic R (by Argenta), which has 12 kW of power. Different casting tools were used in this process, such as a high-density graphite crucible, a molding box and filler sand. To analyze the quality of the aluminum castings, roughness and volumetric porosity were analyzed using the profilometer and the balance mentioned above. In the case of the latter, distilled water was used for hydrostatic weighing [44]. On the other hand, the internal porosity of different sectors of the cast parts was studied. For this purpose, a wafering saw, equipped with a carbide disc, was used. The specimens obtained were polished according to the recommendations of the ASTM E3 standard [45]. Then, different images of the polished sections were analyzed. These images were acquired using an Olympus BHM metallographic optical microscope and analyzed with ImageJ image analysis software.

3.2. Methods

3.2.1. Cube specimens

With the aim of evaluating the variations of the 3D printed parts throughout the steps of the presented procedure (in terms of weight, dimensions, porosity, surface quality and compressive strength), a 40 mm-sided cube was designed, see Fig. 2. This design followed the recommendations of the standards ISO 679 [42] and ASTM C373–88 [40], in terms of the dimensions and minimum weight required to evaluate the strength of the material and its volumetric porosity. In addition, these specimens had a sufficient surface area to meet the recommendations of ISO 4288 [41]. As can be seen in Fig. 2, the designed specimen was marked, in order to be able to identify the specific specimen, its orientation with respect to the machine axes and the directions for roughness measurement, (R_1, R_2 and R_3).

The procedure presented in this work has four steps of material treatment, as described above. Based on the changes that the material undergoes during this process, three conditions can be defined, apart from the original stage after manufacturing (As-built):

- As-built (AB);
- After the first drying HT ($1D_{HT}$);
- After infiltration and capillary humidity removal HT (IHR);
- After the second drying HT ($2D_{HT}$).

It should be noted that no condition was defined for the material immediately after the infiltration process. This is because, in that moment, the material contained a high proportion of water, which

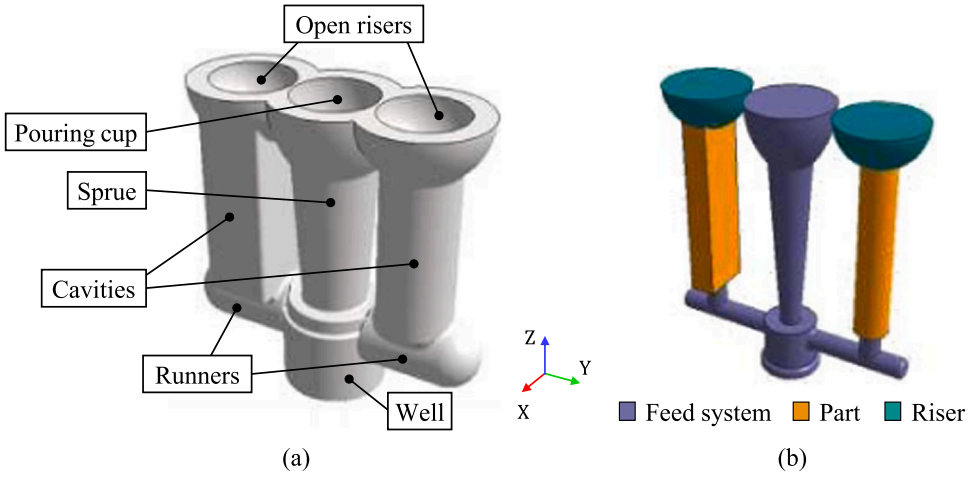

Fig. 4. Case study mold design: (a) mold, (b) casting volume.

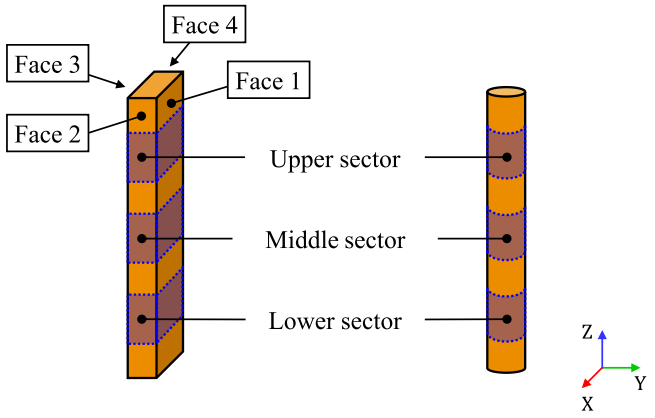

Fig. 5. Analysis sectors of the specimens.

makes its mechanical properties very poor. This decrease in properties can be explained by the high degree of solubility of calcium sulfate in water. Thus, in order to recover acceptable mechanical properties of the material, a heat treatment is mandatory, after which the material achieves the IHR condition.

To analyze the conditions of the 3D printed parts, various sets were manufactured, each one comprising four cubic specimens with the same machine configuration and at the same position within the machine volume. For each set, three cubes were submitted to a compression test by applying the load in the Z direction, see Fig. 2. The roughness was measured on the XY, YZ and XZ faces of the fourth cube, following directions marked R1, R2, and R3, see Fig. 2a. For this purpose, five homogeneously distributed profiles were captured in the indicated direction for each face, obtaining the mean value of the Ra and Rt roughness parameters. Then, an Archimedes method test was performed on this cube to determine its bulk density. This cube was discarded for the compression test, due to the liquid absorbed during the last test.

With the aim of determining the properties of the material through the procedure presented, three plus three sets of cubes were manufactured. The former three sets were analyzed in the As-built, $1D_{HT}$ and IHR conditions, one set per condition. The latter three sets were analyzed once the procedure was applied but using different temperatures for the *second drying HT*: 150, 175 and 200 °C ($2D_{HT}^{150}$, $2D_{HT}^{175}$, $2D_{HT}^{200}$). Therefore, a total of six sets of cubes were analyzed, i.e. 24 cubes in total. This process is illustrated in Fig. 3. It is important to note that the dimensions and weights of all the cubes were analyzed for all the conditions during the procedure, due to the non-destructive nature of the required tests.

3.2.2. Case study

With the aim of demonstrating the value of the procedure, a practical case was defined and applied to 3D printed parts, to be used as expendable tools in metal casting processes. An aluminum casting was performed using a 3D printed mold treated with this procedure. The quality of the aluminum part was compared with the quality of the same part obtained with a mold without any type of treatment: an as-built mold. This quality was analyzed in terms of roughness and volumetric and internal porosity. The temperature used in the second drying of the treated mold was 175 °C ($2D_{HT}^{175}$ condition).

The ad-hoc designed mold consisted of a vertical feeding system comprising a cup, a sprue and a well, the latter connected by two horizontal runners to two cavities on both sides, see Fig. 4. To facilitate the analysis of the quality of the parts obtained with this mold, the cavities consisted of two simple three-dimensional geometries for different purposes: a parallelepiped with a section 12 × 24 mm^2 for the roughness analysis and a cylinder of 16 mm diameter for the porosity analysis; both had a height of 90 mm. Semi-spherical risers were designed at the top of each cavity to compensate the metal shrinkage during solidification, so that any defects observed in the obtained parts could only be attributed to the release of volatiles from the mold during the pouring process. This mold had a wall thickness of 10 mm and an approximate mass of 130 g.

The aluminum gravity pouring process was carried out following an identical procedure for both molds. In both cases, a molten aluminum mass of 500 g was used. The pouring temperature was 730 °C ± 5 °C with a holding time of 2 min. After solidification, the mold was carefully removed manually and the parts were separated from the rest of the casting using a metal saw.

The surface roughness of the parallelepiped molded parts was analyzed in three different sectors, distributed along their heights and on all four faces, see Fig. 5. Three roughness profiles in the vertical direction were collected on each sector of these faces. The roughness parameter Ra was obtained using a λ_c of 2.5 mm and λ_s of 8 μm, according to ISO 4288 [41].

On the other hand, the porosity of casted parts was analyzed using cylindrical specimens in two phases. First, a hydrostatic weighing method was used to determine their actual density and, consequently, their volumetric porosity [43,46]. Then, three sectors (distributed along its height, Z), were extracted for internal porosity analysis. From these extracted sectors of the cylinder, the upper surfaces were polished following the indications of the ASTM E3 standard [45]. These surfaces coincide with the orientation of the XY plane. Subsequently, a 50 image matrix arrangement was taken using the optical microscope, covering the total of each polished surface. These images were processed with ImageJ software. From this set of images, pores were identified by adjusting a threshold filter. The number, size and shape of these pores were analyzed according to the sector of the piece in which they were

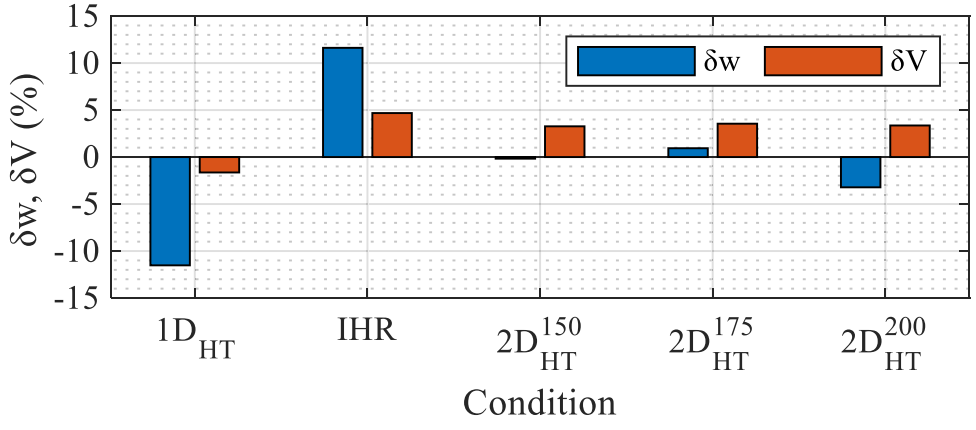

Fig. 6. Weight and Volume of the cubes in the different conditions, with regard to the AB condition.

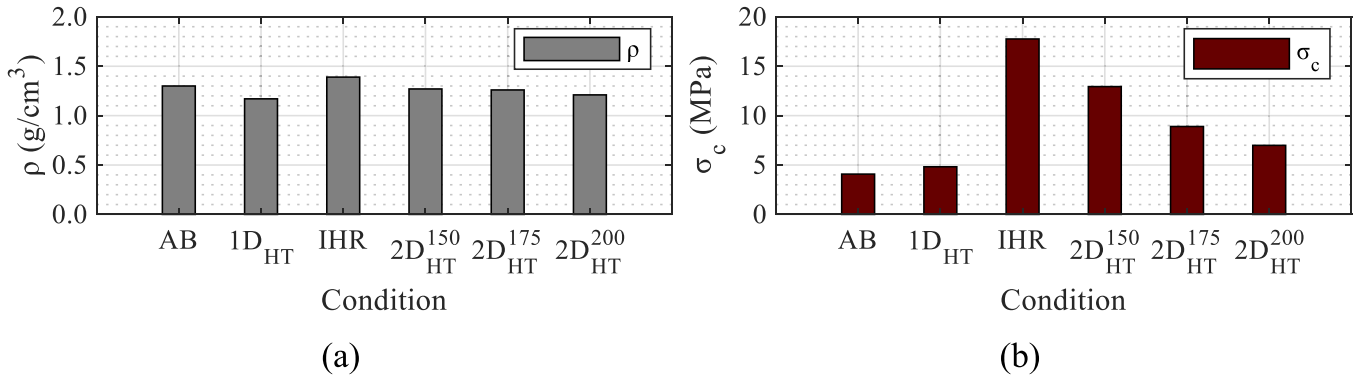

Fig. 7. Apparent density (a) and Compression strength (b) in the different conditions.

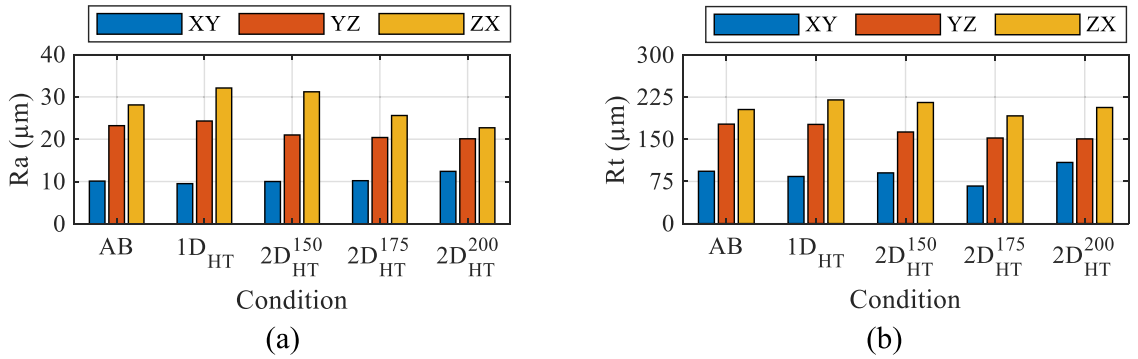

Fig. 8. Ra (a) and Rt (b) detected in different final conditions.

found. Their size was analyzed using Feret's maximum diameter, while their shape was analyzed using an aspect ratio, based on the ratio between Feret's minimum and maximum diameters.

3. Results and discussion

In this section, the changes observed in the properties of cubic specimens at the different steps of the procedure are presented and analyzed. In addition, differences in the observed properties between a casting part manufactured with a mold treated with the developed procedure and another part manufactured with a mold directly from the AM machine are discussed.

3.1. Cube specimens

Fig. 6 shows the average results obtained for weight and apparent volume of the sets of cubes for the different conditions, with respect to the initial condition of the material (AB). In the cases of the intermediate conditions at which the weight and dimensions were recorded (Fig. 3), the results were averaged with those values of the cubes for which that condition was the final condition. This means that the values in Fig. 6, for stage $1D_{HT}$, were obtained as the average of 20 cubes, and those for IHR were the average of 16 cubes, etc. Observing these results, it can be seen that the material changes in weight and volume throughout the procedure. When the material undergoes heat treatment, it loses water, reducing its weight and volume. After infiltration, the material gains weight, due to the absorbed infiltrant, and it also increases in volume. The weight acquired by the infiltrant reduces with the second drying. The volume slightly reduces, to a lesser extent, than the weight.

Fig. 7a shows the bulk density obtained in the different conditions. There are small fluctuations, with the density increasing with infiltration and decreasing with the different heat treatments. The final material bulk density, after the last treatment, is slightly lower than the initial one. Although this density information could be related to porosity, no conclusive results have been obtained in this study. It is recommended that higher weight specimens are used. Despite complying with the minimum weight required by the ASTM C373–88 standard [40], the uncertainty in the measurement did not allow this relationship to be identified in the present work.

On the other hand, Fig. 7b shows the compressive strength obtained for the cubes in the different conditions. With the first drying heat treatment, the strength increases from 4.08 to 4.82 MPa (18%). The increase in strength is due to the binder removal, which is in line with the basic treatment recommended by the manufacturer. After the infiltration process and the capillary humidity removal heat treatment (IHR) a maximum strength of 17.76 MPa was detected. This implies an increase of 335%, with respect to the initial condition. This strength is also much higher than that obtained by other workers [31], of the order of 150%, that used the same material and infiltrant but followed the recommendations of the material supplier. This is due to both the high penetration of the infiltrant achieved with the proposed vacuum technique and the improved setting of the calcium sulfate - magnesium sulfate mixture achieved, with the proposed capillary humidity removal HT. Both aspects are innovations of the presented procedure.

Regarding the second drying heat treatment, rather than improving the strength further, it negatively affected it. This was due to the generation of γ-anhydrite by the calcium sulfate. The higher the temperature of this treatment, the higher the proportion of this phase that was formed and, therefore, the lower the strength will be. In any case, it should be noted that, on the one hand, even using a temperature of 200 °C the resistance increased by 71% with respect to the AB condition. On the other hand, the higher the temperature, the more water was removed from the material, which implies a better applicability to high temperature processes such as the casting processes. Therefore, a balance between strength and water content will have to be found for each specific application.

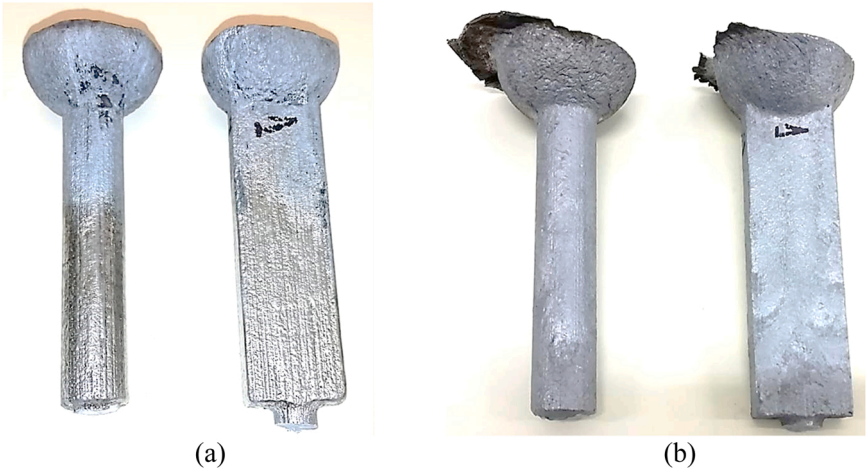

Fig. 9. Molded parts using different molds: (a) as-built mold, (b) treated mold.

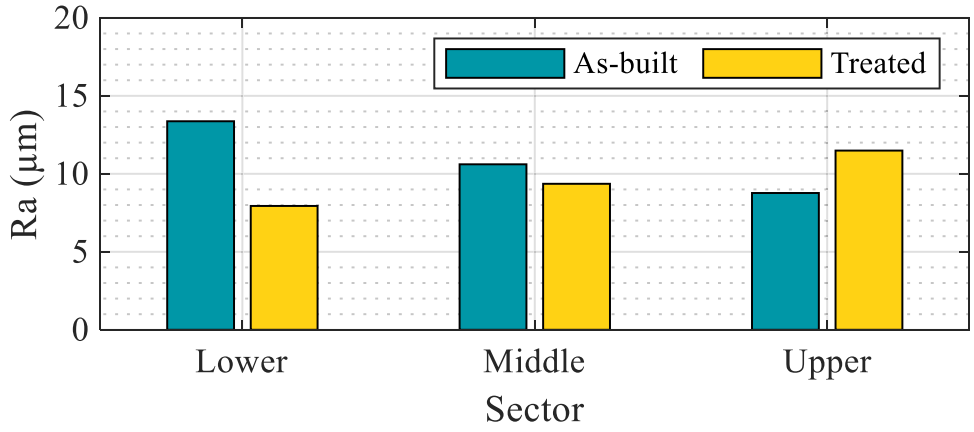

Fig. 10. Ra values for the specimens obtained using as-built and treated molds.

The roughness results for the different conditions are shown in Fig. 8. As can be seen by observing the results obtained for the Ra parameter (Fig. 8a), the roughness on the top face of the cube, XY, is lower than those on the vertical faces, YZ and ZX. The one with the worst roughness is the ZX face. Regarding the effect of the procedure on the roughness, it should be noted that it does not practically alter in the XY face, decreasing slightly in the YZ face and more significantly in the ZX face, especially the last heat treatment. Regarding the Rt parameter (Fig. 8b), a similar effect to Ra is observed, although with a less significant improvement after the second heat treatment. This may be due the Rt parameter, unlike Ra, being obtained from individual height values of the roughness profile. Thus, small protuberances adhered to the surface of the material after the second heat treatment, derived from the expulsion of volatiles in the form of bubbles, which may be the reason why the improvement is not as marked as in the case of the Ra parameter. In any case, in general, the Rt values after the procedure are better than those shown by the material at the beginning, i.e. AB condition.

3.1.1. *Case study*

Fig. 9 shows the parts obtained with the as-built mold and with the treated mold. As shown, surfaces of the parts obtained with the as-built mold are shinier and more textured (Fig. 9a) than those of the parts obtained with the treated mold (Fig. 9b).

Fig. 10 shows the results for the average Ra value, measured at the

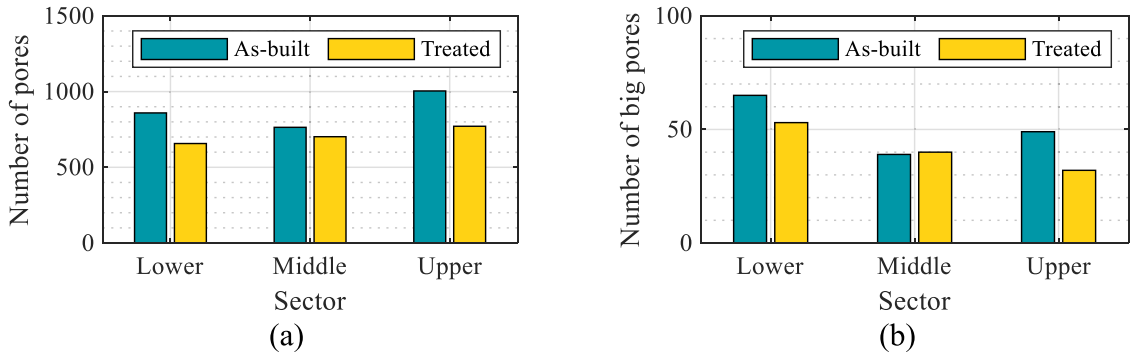

Fig. 11. Number of pores detected for the specimens obtained with the as-built and treated molds: (a) pores, (b) large pores (Max Feret diameter $\geq$ 90 µm).

Table 5
Size and aspect ratio of pores detected in the different sectors of the parts obtained with both molds.

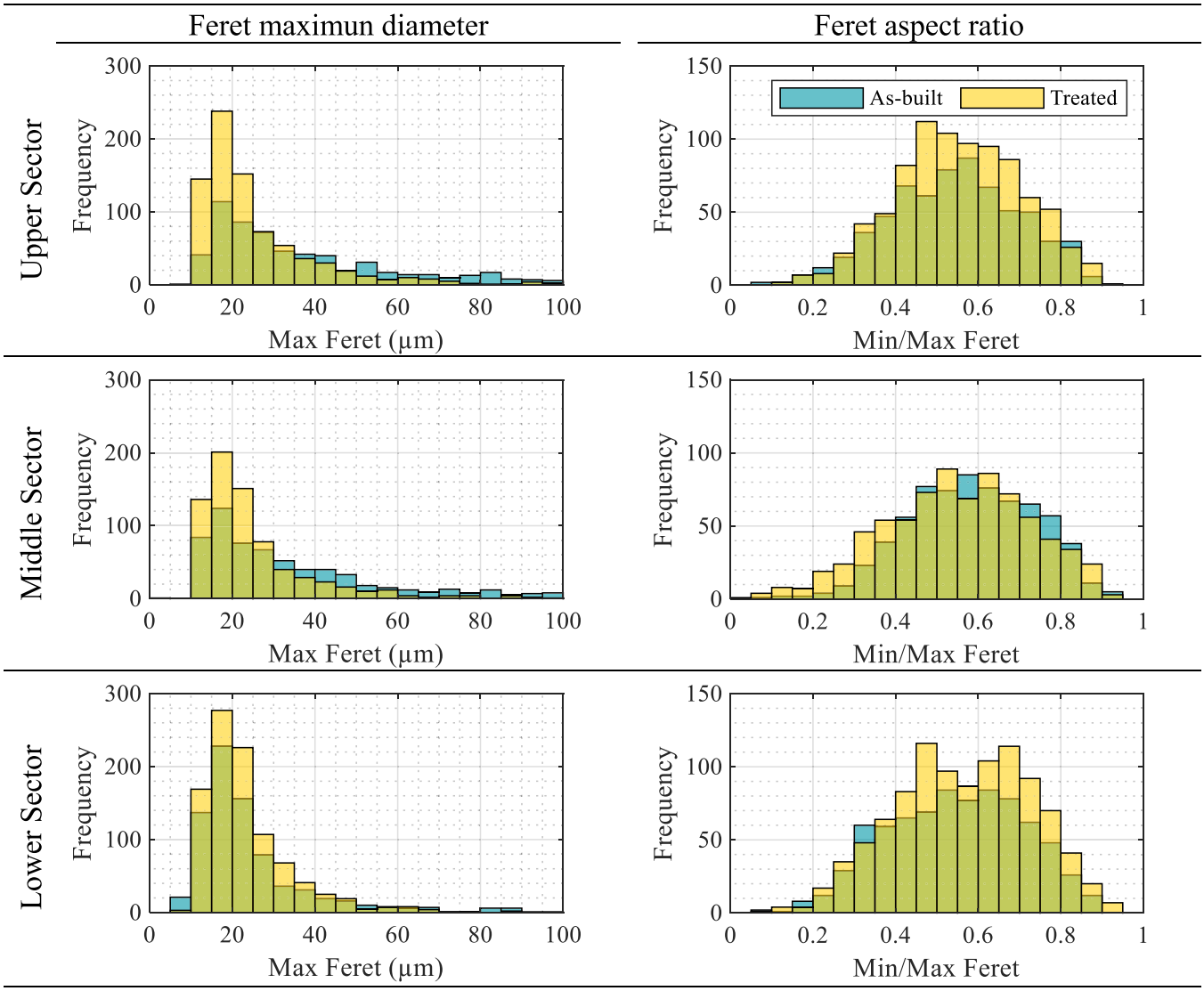

different sectors for the parallelepiped parts obtained with both molds. In the case of the part obtained with the as-built mold, the roughness increases with the vertical position, being 13.37 μm in the lower sector, 10.61 μm in the middle and 8.77 μm in the upper one. This could be related to the trapping of volatile bubbles between the surface of the solidified material and the mold wall.

Gases are generated during the pouring of the liquid metal due to the low melting point compounds contained in the mold, mainly binder in this case. These gases cannot escape to outside due to the low permeability of the mold material, so they are expelled into the cavity where they interact with the liquid metal. A portion of these volatiles escape to the atmosphere when the mold filling is incomplete. However, when the mold cavity is filled with molten metal, due to surface tension these gases form bubbles that can be trapped inside the metal or between the metal and the mold, if they cannot float and escape to the atmosphere before the metal has completely solidified. The trend observed in the roughness of the part produced with the as-built mold indicates that the volatiles expelled from the bottom of the mold had more difficulty in escaping to the outside and, therefore, the surface quality worsens the deeper the sector is analyzed. This is due to the greater distance that the volatile gas bubbles must travel before escaping through the area of the risers and the higher metallostatic pressure to which they are subjected.

Regarding the roughness of the part manufactured by means of the treated mold, 7.94 μm were obtained in the lower sector, 9.36 μm in the middle and 11.49 μm in the upper one. Despite the fact that the roughness trend is inverse to that observed for the part obtained with the as-built mold, the range is lower in this case: 3.55 μm compared to 4.60 μm. Moreover, in both the lower and middle sectors, the roughness of the part obtained with the treated mold is finer; differences of 5.43 μm and 0.88 μm were detected for the lower and middle sectors, respectively. Therefore, it can be stated that the roughness of the part obtained with the treated mold is generally finer and more homogeneous than that obtained with the as-built mold. This actually coincides with what was observed by the visual examination of both parts, see Fig. 9.

The difference in roughness can be transferred to a difference in surface porosity and, consequently, to a combination of differences in the volatile content and permeability of the analyzed molds. The moisture content of the treated mold is lower, which in turn improves its permeability [34,35]. The results obtained for the volumetric porosity of the parts also point in this direction: 3.53% for the cylinder obtained with the as-built mold, 1.80% for the one obtained with the treated mold.

Regarding the internal porosity, Fig. 11a shows the presence of internal pores in the different analyzed sectors of the cylindrical parts for both molds. The number of pores is lower and more uniform in the sectors of the part obtained with the treated mold than in that obtained

Table 6
Typical pores found in the analyzed sectors of the parts obtained with both molds.

Mold	Sector: Lower	Sector: Middle	Sector: Upper
As-built	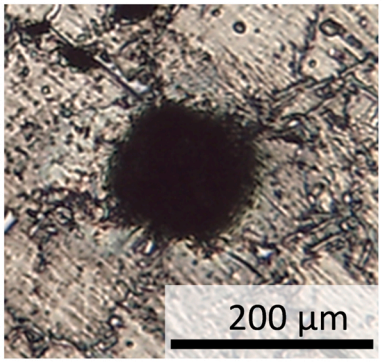	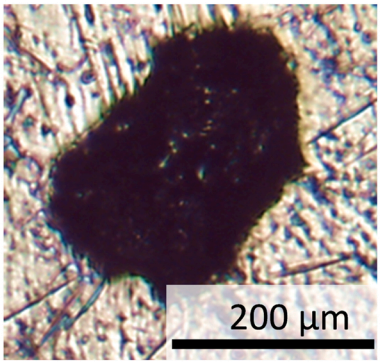	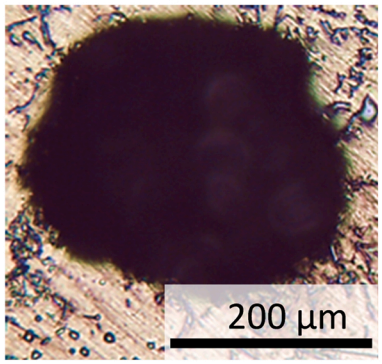
Treated	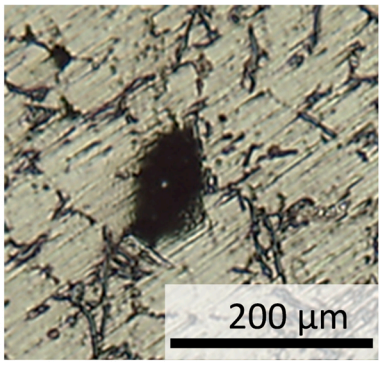	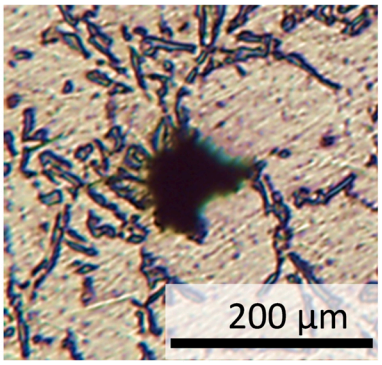	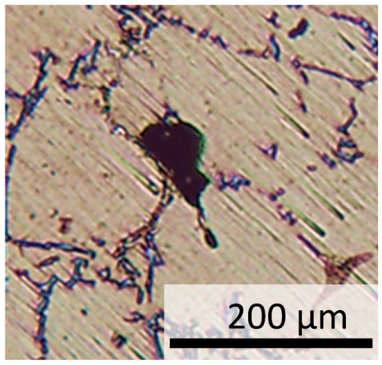

with the as-built mold. Similar behavior is observed for the most problematic (larger) pores, with a maximum Feret diameter of more than 90 µm, see Fig. 11b. In all cases, these large pores account for less than 9% of the total found in each sector. The lower porosity detected in the part obtained with the treated mold can be related to a lower expulsion of volatiles in this mold, due to both a reduction of the moisture content and an improvement in its permeability.

Regarding pore size distribution and pore shape, histograms of maximum Feret diameter and pore aspect ratio are shown in Table 5. As can be seen in the left column, size distribution is similar in the two parts and in the three sectors, although the pore diameters in the part obtained with the treated mold are more concentrated around the mode of the distribution, i.e. 15–20 µm.

Regarding pore shape, the right hand column of Table 5 shows the aspect ratio. It is similar in the two parts in the three sectors analyzed (an average value of approximately 0.6). The fact that this value is above 0.5 indicates that pores are predominantly spherical, reaffirming that the amount of volatiles contained and expelled by the treated mold is lower than that of the as-built mold. Table 6 shows pores found in the parts and sectors analyzed, where it is possible to appreciate their round shape instead of elongated or crack-shapes. This indicates that they have been formed by the accumulation of gas bubbles and not by the effect of the material shrinkage.

5. Conclusions

This work presents a novel post-processing procedure for parts made of calcium sulfate using the binder jetting additive manufacturing technique. This post-processing increases the compressive strength and reduces the moisture content, thus improving the applicability as expendable elements, i.e. molds, cores, etc., in metal casting processes. This procedure consists of the application of different thermal treatments in combination with a vacuum infiltration process of a solution of magnesium sulfate heptahydrate (Epsom salt) in distilled water. Unlike the furans commonly used in the manufacture of plaster molds, Epsom salt is a compound that is harmless to health and the environment. The post-process is applied to the parts manufactured by BJ from their as-built condition, AB, in four steps:

1. First drying HT: heat treatment at 80 °C for 2 h that allows the gypsum to revert to its hemihydrated state, preparing the material for the subsequent infiltration process without losing its shape. After this treatment, the material acquires the $1D_{HT}$ condition.
2. Infiltration: infiltration of magnesium sulfate solution in distilled water at maximum solubility, applying an absolute pressure of 150 mbar for 1 min, which reverts the gypsum to a dihydrated state and allows magnesium sulfate heptahydrate to be diffused deep into the interior of the material.
3. Capillary humidity removal HT: heat treatment at 80 °C for 24 h to remove the excess of humidity acquired during infiltration, non-crystallization water, and preparing the material for the next step. After this treatment, the material acquires the IHR condition.
4. Second drying HT: heat treatment between 150 and 200 °C for 6 h, to remove moisture from the material, preventing the formation of γ-anhydrite. The higher the temperature, the more moisture will be removed, but the higher proportion of γ-anhydrite will be generated, which reduces the material strength. After this treatment, the material acquires the $2D_{HT}$ condition.

Tests on cubic specimens according to the ISO 679 and ASTM C373–88 standards led to the following conclusions:

- Weight and volume: they vary for the different conditions due to the mass gain during the infiltration and moisture loss with

heat treatments. In the last condition, $2D_{HT}$, mass and volume are similar to the initial, condition AB. This is interesting for applying this method to molds as they maintain their geometry after the procedure.

- Density: it varies slightly in the different states but reaches a value similar to the initial one once the procedure is completed. Due to the small variation observed and the uncertainties in the measurement, the results could not be related to the porosity of the specimens. In order to do this, larger specimens or more accurate equipment is recommended.
- Compressive strength: the strength of the material in the initial condition, AB, is lower than that shown in all the conditions throughout the post-processing procedure, $1D_{HT}$, IHR, $2D_{HT}$. The maximum strength is achieved in the IHR condition, 335% higher than the original. Since, in this condition, the material still contains a large amount of moisture, in the case of using the part as an expendable element in metal casting, it is recommended that the last heat treatment is performed, allowing it to reduce the moisture content. The temperature that removes the most amount of moisture, 200 °C ($2D_{HT}^{200}$), allows an increase in strength of 71% with respect to the original condition, AB.
- Roughness: an improvement in the parameters Ra and Rt is observed, more marked in the latter. This relates to the finer roughness observed in the mold material.

After analyzing the effect of the presented post-processing on the material, it was applied to a case study of AlSi7Mg aluminum alloy casting with an ad-hoc mold design. The quality of the part manufactured using an untreated mold (as-built) was compared to that manufactured using the same mold design but treated with the presented procedure. From this comparison, it is concluded that part roughness is finer and more homogeneous with the treated mold. Also, volumetric and internal porosities are lower in the case of parts obtained with the treated mold. Therefore, it can be affirmed that the proposed procedure allows reducing the moisture content of this type of BJ parts, improving their permeability and reducing the amount of volatiles retained in the parts during the foundry process.

In conclusion, it can be stated that the procedure presented in this work allows for improving the compressive strength and reducing the volatile content of parts manufactured in gypsum by means of the AM binder jetting technique, without significantly altering their geometry. These facts significantly enhance their applicability to metal casting once the $2D_{HT}$ condition is reached. For other applications, that only require higher compressive strength, regardless of moisture content, the presented procedure allows a four-fold increase in compressive strength once the IHR condition is reached, with regard to the as-built parts. These results substantially improve on those obtained using the infiltration process currently recommended by the supplier of the 3Dsystem.

Limitations of the developed procedure include the possible deterioration of thin areas when it is applied to parts with different thickness as well as the need for different auxiliary equipment to apply it. Therefore, future challenges include the optimization of the procedure depending on the complexity and the size of the part, as well as the development of specific equipment to simplify its application, which could be integrated into the AM machines themselves in the future.

CRediT authorship contribution statement

Pablo Rodríguez-González: Writing – original draft, Methodology, Formal analysis, Conceptualization. **Pablo Zapico:** Writing – review & editing, Methodology, Formal analysis, Conceptualization. **Pablo Eduardo Robles-Valero:** Methodology, Investigation, Conceptualization. **Joaquín Barreiro:** Writing – review & editing, Supervision, Resources, Project administration.

Declaration of Competing Interest

The authors declare that they have no known competing financial interests or personal relationships that could have appeared to influence the work reported in this paper.

Data Availability

Data will be made available on request.

Acknowledgements

This work was supported by the Spanish Ministry of Science, Innovation and Universities and FEDER, through a research project with the reference DPI2017–89840-R.

References

[1] I. Campbell, D. Bourell, I. Gibson, Additive manufacturing: rapid prototyping comes of age, Rapid Prototyp. J. 18 (2012) 255–258, https://doi.org/10.1108/13552541211231563.
[2] Wholers Report, Wholers Associates, Fort Collins, CO, 2019.
[3] M. Attaran, The rise of 3-D printing: the advantages of additive manufacturing over traditional manufacturing, Bus. Horiz. 60 (2017) 677–688, https://doi.org/10.1016/j.bushor.2017.05.011.
[4] S.H. Huang, P. Liu, A. Mokasdar, L. Hou, Additive manufacturing and its societal impact: a literature review, Int. J. Adv. Manuf. Technol. 67 (2013) 1191–1203, https://doi.org/10.1007/s00170-012-4558-5.
[5] H. Bikas, A.K. Lianos, P. Stavropoulos, A design framework for additive manufacturing, Int. J. Adv. Manuf. Technol. 103 (2019) 3769–3783, https://doi.org/10.1007/s00170-019-03627-z.
[6] P. Stavropoulos, P. Foteinopoulos, A. Papapacharalampopoulos, On the impact of additive manufacturing processes complexity on modelling, Appl. Sci. 11 (2021) 7743, https://doi.org/10.3390/app11167743.
[7] ISO, ISO/ ASTM 52900:2015, Additive Manufacturing - General Principles - Terminology), International Organization for Standardization, 2015.
[8] B. Derby, Additive manufacture of ceramics components by inkjet printing, Engineering 1 (2015) 113–123, https://doi.org/10.15302/J-ENG-2015014.
[9] P. Stavropoulos, P. Foteinopoulos, Modelling of additive manufacturing processes: a review and classification, Manuf. Rev. 5 (2018) 2, https://doi.org/10.1051/mfreview/2017014.
[10] H. Bikas, P. Stavropoulos, G. Chryssolouris, Additive manufacturing methods and modelling approaches: a critical review, Int. J. Adv. Manuf. Technol. 83 (2016) 389–405, https://doi.org/10.1007/s00170-015-7576-2.
[11] P. Rodríguez-González, A.I. Fernández-Abia, M.A. Castro-Sastre, J. Barreiro, Heat treatments for improved quality binder jetted molds for casting aluminum alloys, Addit. Manuf. 36 (2020), 101524, https://doi.org/10.1016/j.addma.2020.101524.
[12] K.J. Hodder, R.J. Chalaturnyk, Bridging additive manufacturing and sand casting: Utilizing foundry sand, Addit. Manuf. 28 (2019) 649–660, https://doi.org/10.1016/j.addma.2019.06.008.
[13] S. Huang, C. Ye, H. Zhao, Z. Fan, Additive manufacturing of thin alumina ceramic cores using binder-jetting, Addit. Manuf. 29 (2019), 100802, https://doi.org/10.1016/j.addma.2019.100802.
[14] E. Bassoli, E. Atzeni, Direct metal rapid casting: mechanical optimization and tolerance calculation, Rapid Prototyp. J. 15 (2009) 238–243, https://doi.org/10.1108/13552540910979758.
[15] T.J. Ayres, S.R. Sama, S.B. Joshi, G.P. Manogharan, Influence of resin infiltrants on mechanical and thermal performance in plaster binder jetting additive manufacturing, Addit. Manuf. 30 (2019), 100885, https://doi.org/10.1016/j.addma.2019.100885.
[16] R.N. Lumley, Aluminum Investment Casting and Rapid Prototyping for Aerospace Applications, Elsevier Ltd, 2018, https://doi.org/10.1016/b978-0-08-102063-0.00004-7.
[17] A. Butscher, M. Bohner, C. Roth, A. Ernstberger, R. Heuberger, N. Doebelin, P. Rudolf Von Rohr, R. Müller, Printability of calcium phosphate powders for three-dimensional printing of tissue engineering scaffolds, Acta Biomater. 8 (2012) 373–385, https://doi.org/10.1016/j.actbio.2011.08.027.
[18] A. Farzadi, M. Solati-Hashjin, M. Asadi-Eydivand, N.A.A. Osman, Effect of layer thickness and printing orientation on mechanical properties and dimensional accuracy of 3D printed porous samples for bone tissue engineering, PLoS One 9 (2014) 1–14, https://doi.org/10.1371/journal.pone.0108252.
[19] A. Mostafaei, E.L. Stevens, J.J. Ference, D.E. Schmidt, M. Chmielus, Binder jetting of a complex-shaped metal partial denture framework, Addit. Manuf. 21 (2018) 63–68, https://doi.org/10.1016/j.addma.2018.02.014.
[20] J. Wu Kang, Q.Xian Ma, The role and impact of 3D printing technologies in casting, China Foundry 14 (2017) 157–168, https://doi.org/10.1007/s41230-017-6109-z.
[21] Z. Chen, Z. Li, J. Li, C. Liu, C. Lao, Y. Fu, C. Liu, Y. Li, P. Wang, Y. He, 3D printing of ceramics: a review, J. Eur. Ceram. Soc. 39 (2019) 661–687, https://doi.org/10.1016/j.jeurceramsoc.2018.11.013.

[22] M. Upadhyay, T. Sivarupan, M. El Mansori, 3D printing for rapid sand casting—a review, J. Manuf. Process. 29 (2017) 211–220, https://doi.org/10.1016/j.jmapro.2017.07.017.
[23] E. Bassoli, A. Gatto, L. Juliano, M.G. Violante, 3D printing technique applied to rapid casting, Rapid Prototyp. J. 3 (2007) 148–155, https://doi.org/10.1108/13552540710750898.
[24] Y. Huang, M.C. Leu, J. Mazumder, A. Donmez, Additive manufacturing: current state, future potential, gaps and needs, and recommendations, J. Manuf. Sci. Eng. 137 (2015), 014001, https://doi.org/10.1115/1.4028725.
[25] E.S. Almaghariz, B.P. Conner, L. Lenner, R. Gullapalli, G.P. Manogharan, B. Lamoncha, M. Fang, Quantifying the role of part design complexity in using 3d sand printing for molds and cores, Int. J. Met. 10 (2016) 240–252, https://doi.org/10.1007/s40962-016-0027-5.
[26] D.A. Snelling, R. Kay, A. Druschitz, C.B. Williams, Mitigating gas defects in castings produced from 3D printed molds, In 117th Metalcasting Congress (2012).
[27] S.G. Acharya, J.A. Vadher, P.V. Kanjariya, Identification and quantification of gases releasing from furan no bake binder, Arch. Foundry Eng. 16 (2016) 5–10.
[28] P. Rodríguez-González, P.E.R. Valero, A.I. Fernández-Abia, M.Á. Castro-Sastre, J. B. García, Feasibility of calcium sulfate molds made by inkjet 3D printing for rapid casting of aluminum alloys, Met. (Basel) 10 (2020) 1–17, https://doi.org/10.3390/met10060802.
[29] M. Vlasea, E. Toyserkani, R. Pilliar, Effect of gray scale binder levels on additive manufacturing of porous scaffolds with heterogeneous properties, Int. J. Appl. Ceram. Technol. 12 (2015) 62–70, https://doi.org/10.1111/ijac.12316.
[30] M. Ziaee, N.B. Crane, Binder jetting: a review of process, materials, and methods, Addit. Manuf. 28 (2019) 781–801, https://doi.org/10.1016/j.addma.2019.05.031.
[31] A.D. Ledingham, J.D. English, S. Akyalcin, B.E. Cozad, J.C. Ontiveros, F.K. Kasper, Accuracy and mechanical properties of orthodontic models printed 3-dimensionally from calcium sulfate before and after various postprinting treatments, Am. J. Orthod. Dentofac. Orthop. 150 (2016) 1056–1062, https://doi.org/10.1016/j.ajodo.2016.04.027.
[32] D. Impens, R.J. Urbanic, A comprehensive assessment on the impact of post-processing variables on tensile, compressive and bending characteristics for 3D printed components, Rapid Prototyp. J. 22 (2016) 591–608, https://doi.org/10.1108/RPJ-02-2015-0018.
[33] P. Stavropoulos, P. Foteinopoulos, A. Papacharalampopoulos, H. Bikas, Addressing the challenges for the industrial application of additive manufacturing: Towards a hybrid solution, Int. J. Lightweight Mater. Manuf. 1 (2018) 157–168, https://doi.org/10.1016/j.ijlmm.2018.07.002.
[34] S. Kalpakjian, S.R. Schmid. Manufacturing Engineering & Technology, seventh ed., Pearson, 2014.
[35] R. Singh, Chapter 12 – Mold and Core Making in: Introduction to basic manufacturing processes and workshop technology, New Age International, New Delhi, 2006, pp. 208–241.
[36] M. Yan, H. Takahashi, Effects of magnesia and potassium sulfate on gypsum-bonded alumina dental investment for high-fusing casting, Dent. Mater. J. 17 (4) (1998) 301–313, https://doi.org/10.4012/dmj.17.301.
[37] 3D Systems, Instructions for Salt Water Cure. http://infocenter.3dsystems.com/projetcjpx60/ post-processing-guide/post-processing-part/user-guide-visijet%C2%AE-pxl/appendix/ instructions-salt-water. (Accessed 15 February 2021).
[38] R.C. Ropp, - Group 16 (O, S, Se, Te) Alkaline Earth Compounds, in: R.C. Ropp (Ed.), Encycl. Alkaline Earth Compd, Elsevier, Amsterdam, 2013, pp. 105–197, https://doi.org/10.1016/B978-0-444-59550-8.00003-X.
[39] 3D Systems, Inc, 3D Systems Colorjet Printing Brochure Brilliant full-color parts with ProJet® CJP x60 3D, v02–17., Rock Hill, SC (2017).
[40] A.S.T.M. ASTM, C373-88, Test Method for Water Absorption, Bulk Density. Apparent Porosity, and Apparent Specific Gravity of Fired Whiteware Products, American Society for Testing and Materials, 2006.
[41] ISO, ISO 4288, 1996, Geometrical Product Specifications (GPS) — Surface Texture: Profile Method — Rules and Procedures for the Assessment of Surface Texture, International Organization for Standardization, 1996.
[42] ISO, ISO 679, 2009, Cement - Test Methods - Determination of Strength, International Organization for Standardization, 2009.
[43] CEN, EN 1706:2011, Aluminum and Aluminum Alloys - Castings - Chemical Composition and Mechanical Properties, European Committee for Standardization, 2011.
[44] H. Cao, M. Hao, C. Shen, P. Liang, The influence of different vacuum degree on the porosity and mechanical properties of aluminum die casting, Vacuum 146 (2017) 278–281, https://doi.org/10.1016/j.vacuum.2017.09.048.
[45] A.S.T.M. ASTM, E3-01, Guide for Preparation of Metallographic Specimens ASTM International, American Society for Testing and Materials, 2017.
[46] N.A. Pratten, The precise measurement of the density of small samples, J. Mater. Sci. 16 (1981) 1737–1747, https://doi.org/10.1007/BF00540619.